Acoustics 2021
Wollongong, Australia
MAKING WAVES
8 - 10 November

An analytical and experimental study of railway noise emissions from Sydney Harbour Bridge

Graham Brown (1), David Timms (1), Peter Lark (2) and Ross Emslie (2)

(1) Engineering Sciences, Mott Macdonald, Sydney
(2) Advanced Analysis and Test, Jacobs, Sydney

ABSTRACT

An analysis of noise generated from railway operations on Sydney Harbour Bridge is presented based on a hybrid analytical and experimental method. The approach includes vibro-acoustic testing of the rails, rail deck and supporting structures. The receptance of the rails and rail supports is determined along with the rail vibration decay rate. Measurements of operational vibration on the rails and at a matrix of locations on the bridge structure are used to quantify the energy averaged vibration velocity for each bridge component. The data gathered from testing is used to validate Finite Element and Statistical Energy Analysis models and to calculate the sound power contributions of the train wheels, rails and bridge components. The validated models are used to predict the change in component and overall sound power levels due to the replacement of the pre-existing timber transom rail deck and timber walkways with a low-maintenance continuous concrete rail deck.

1 INTRODUCTION

The timber transom and timber walkway rail deck, which had been a feature of the Sydney Harbour Bridge since opening in 1932, was replaced in January 2021 using a new concrete rail deck. This paper presents the results of a detailed study of the railway noise emissions from the Sydney Harbour Bridge undertaken prior to replacing the rail deck. The objectives of this study were to quantify and rank the noise sources associated with rail operations on the bridge and to ensure that noise levels would not increase as a result of changes to the deck design.

1.1 Bridge and Rail Deck Configuration

The Sydney Harbour Bridge comprises a main span supported from the main arch of the bridge by hangers attached to deep longitudinal stringers and cross girders at 18 m spans and approach spans supported by shallower stringers and cross girders at 9 m spans in turn supported by steel trusses on stone piers. The northern approach span is curved, while the southern approach span is straight, but otherwise structurally identical.

The rail deck, which is on the western side of the bridge, has two identical tracks. The pre-existing tracks comprised timber transoms with Delkor Egg rail isolators supporting the rails at approximately 500 mm intervals. The timber transoms were loosely bolted to the stringer top flange. The stringers also supported a wooden walkway between and on either side of the two tracks. Figure 1 shows the configuration of the Sydney Harbour Bridge.

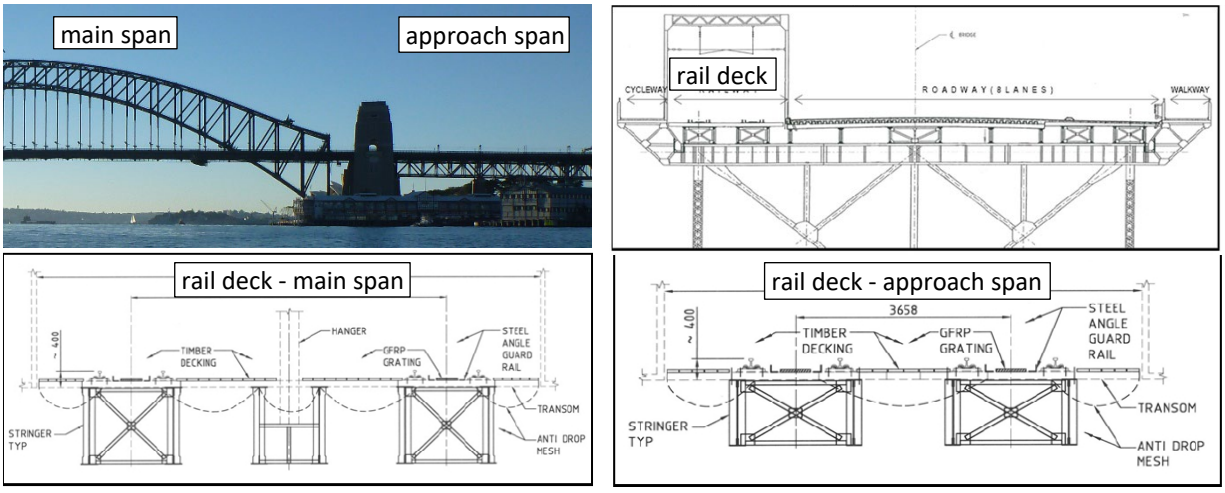

Figure 1: Configuration of Sydney Harbour Bridge main span and approach spans

The new rail deck comprised precast 300 mm thick concrete slabs dowelled and grouted to the stringers and grouted together to form a continuous slab supporting new low profile Delkor Eggs and rails. The track slabs on the approach spans extend to cover the area previously covered by the timber walkway deck.

2 RAIL BRIDGE NOISE GENERATION

Vibration is generated at the wheel/rail interface as a consequence of rolling contact between imperfect wheel and rail surfaces. The vibrating wheels and rails couple to the surrounding air generating noise over a wide frequency band, which radiates into the environment. As shown in Figure 2, part of the rail vibration energy passes through the rail isolator and fastener system and excites the supporting transoms (or future concrete deck elements) which also radiate noise to the surrounds. Vibration energy also passes from the transoms into the stringers and radiates as noise. This process of dispersion of vibration continues through all components connected to the stringers and supporting truss elements throughout the approach spans and the main span of the bridge.

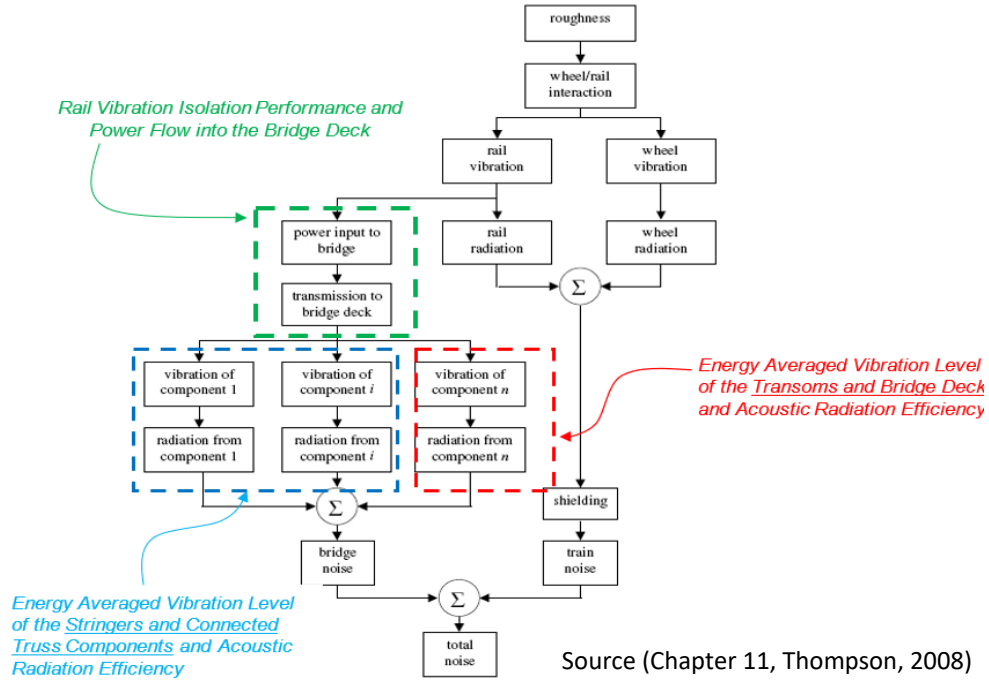

Figure 2: Bridge vibration and noise generation due to train wheel and rail interaction

The extent to which structural vibrations become audible noise is dependent upon the surface area of the vibrating structure and how efficiently the structural vibrations couple with the air. The efficiency of structural vibration translation into noise is described by a frequency-dependent function known as the acoustic radiation ratio or acoustic radiation efficiency. The relationship between sound power and structural vibration is defined by the simple mathematical expression in equation (1) (Bies and Hanson, 2009).

$$W = \rho.c.\sigma.A.\bar{V}^2 \tag{1}$$

where W is the sound power, $\rho.c$ is the impedance of the air, σ is the acoustic radiation efficiency, A is the radiating surface area, and $\bar{V}^2$ is the mean squared surface averaged vibration velocity. The unknown terms in equation (1) are the acoustic radiation efficiency, σ, which can be determined by analytical expressions derived from theory or by use of numerical models; and the vibration velocity, $\bar{V}^2$, which can be determined by measurement for an existing structure, or by use of computer modelling.

Whilst vibration intensity levels throughout the bridge reduce with distance from the wheel/rail interface, the surface area capable of radiating noise to the environment from structure-borne vibration increases substantially. It is therefore important to quantify the contribution from low vibration-large area sources, as it may be similar to or possibly higher than the acoustic power from high vibration-small area sources such as the wheels and rails.

The new concrete deck system was expected to have a higher dynamic stiffness than the existing transoms and therefore likely to improve the vibration isolation performance of the rail isolators and reduce noise radiated from the bridge. However, there was also a risk of an increase in radiated noise due to:

- an increase in total radiating area due to “filling in” spaces between transoms with a continuous plate;
- increased acoustic radiation efficiency of the concrete deck plate compared to the timber transoms;
- changes in the distribution of vibration energy within the bridge structure.

The far field noise spectrum at a reference location 38 m from the nearest rail and 1.5 m above ground level, adjacent to the southern approach span shown in Figure 3. The dominant frequency range is 315 Hz – 1250 Hz. Vibration measurements on the bridge structure suggested that overall far field noise levels from the timber deck bridge were dominated by noise radiated from the bridge structure rather than the direct contribution of wheel and rail noise sources.

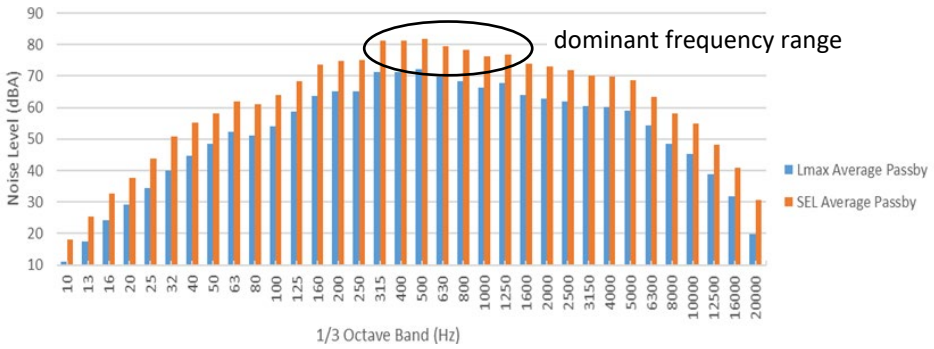

Figure 3: Average rail pas-by sound pressure level (Down track) adjacent southern approach span

3 MODELLING AND TESTING APPROACH

Noise and vibration testing was undertaken in tandem with the development of a vibro-acoustic model of the train wheels and bridge to quantify and rank the contributors to far field noise and predict the change in radiated sound power and sound pressure levels from the concrete deck and the bridge structure. Confidence in predictive models was developed by achieving correlation with measurements of the pre-existing rail deck vibro-acoustic performance before modelling the new deck. Most of the modelling and testing was carried out on the southern approach span of the bridge due to its proximity to noise receivers and the opportunity to access the underside of the rail deck and truss structures at this location.

Measurements consisted of vibration transfer functions, rail roughness and track vibration decay rate and response vibration measurements at a matrix of locations on the bridge and far field sound pressure levels. Driving point and transfer vibration frequency response functions were obtained between rails, baseplates, transoms, and stringers using multi-channel impact testing for locations on the approach and main spans of the bridge. Pass-by vibration data was obtained at 180 measurement locations on the rails, transoms, stringers, cross beams and trusses on the southern approach span. The track vibration decay rate was measured using the method in EN15461 (2008+A1:2010) and rail roughness was measured using a corrugation analysis trolley and EN15610 (2009). Pass-by noise measurements were made at representative far field locations at either end of the bridge. Figure 4 shows images from field testing (left to right): rail receptances, operational vibration and pass-by noise.

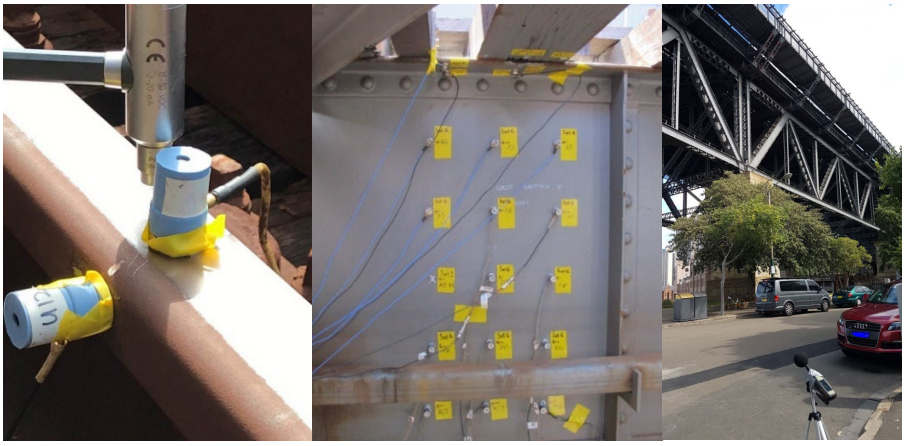

Figure 4: Vibro-acoustic field testing – Sydney Harbour Bridge

Finite Element Analysis (FEA) models of the wheels and rails were used to determine the frequency dependent contact forces at the wheel-rail interface and the vibration isolation performance and vibration power flow for the rail fixings. A detailed FEA model of the wheel was used together with analytical inputs to determine the wheel radiated sound power and FEA and Statistical Energy Analysis (SEA) models of the bridge were used to evaluate bridge radiated sound power.

3.1 Wheel – Rail Interaction Model

FEA models of wheel, rail and track components were created and integrated into a wheel-rail interaction model. The wheel-rail interaction model was used to determine any change in the wheel-rail contact force for the transom/concrete deck configurations due to changing the deck structure. The wheel-rail interaction model provided a means of determining the change in the isolation performance of the rail supports as well as determining the vibration power flow into the bridge structure and the wheel radiated noise contribution.

A direct frequency response analyses was used to determine the individual receptances of the wheel-rail dynamic system components based on the FEA models. The complex receptances were then used as an input to a wheel-rail interaction model as described by Thompson (2008) to predict the wheel-rail contact dynamic force for a unit roughness input.

The relationship between the wheel-rail contact force (F), combined effective wheel-rail roughness ($\emptyset_{\text{roughness}}$) and the component receptances (α) is given by equation (2).

$$F_{Contact} = \frac{\emptyset_{\text{roughness}}}{\alpha_{rail} + \alpha_{wheel} + \alpha_{contact}} \tag{2}$$

Measurements of in-service rail vibration and the track vibration decay rate were used to calibrate the wheel-rail interaction model and to determine the effective combined wheel and rail surface roughness for a representative sample of trains operating on the bridge using the method described by Janssens et. al. (2006). The effective wheel-rail roughness and resultant wheel-rail contact force was also used along with other analytical modelling parameters to determine the radiated noise output from the wheels, which cannot be directly measured.

The predicted receptances were compared to measured receptances on the rails, transoms and stringers to help validate the wheel-rail interaction model.

The wheel dynamic model consists of one eighth of the car body mass and one quarter of a bogie mass connected to primary and secondary suspension spring-damper elements. Movement of the lumped masses is restricted to the vertical direction, being restrained in all other degrees of freedom. The solid wheel is unrestrained other than by its attachment to the half-axle. The half-axle has a symmetry boundary condition at its mid-plane and may rotate (subject to a light rotational resistance) and move vertically at its outboard end. The solid wheel is modelled in detail using solid elements to generate a representative high frequency dynamic response and is excited by a unit dynamic force acting at the wheel-rail contact point. A non-structural mass is added to the inboard side of the wheel on the axle to account for drive and gearbox components on motor cars, providing a total unsprung mass, which is the average of trailer and motor cars. Aspects of the model that are critical to achieving a representative receptance and surface averaged mean square vibration velocity include the inclusion of the axle at frequencies below 1600Hz, a frequency-dependent rolling damping allowance (Thompson, 2008) in addition to the wheel material damping allowance and a fine frequency resolution surrounding resonant peaks.

An important part of the overall modelling strategy was to create the timber transom and concrete deck models using the same types of finite elements and mesh densities. To achieve this, the concrete deck model was created from the timber deck model by infilling the spaces between the timber transoms with elements of a consistent size and changing the deck material properties. This approach leads to increased confidence that any predicted change in the dynamic properties between the two decks is due to a difference in their physical configuration rather than an artifice of the modelling approach.

The track dynamic model consists of five stringer lengths (approximately 50 m of rail). Three of the stringers are modelled in detail using shell elements. The end stringers were represented using highly damped spring elements to simulate the radiation damping associate with connected structural components. There are some approximations involved in this form of model in comparison to an infinite periodic structure model, which need to be accounted for in post-processing but it has the advantage of being implemented in a standard finite element software package.

The wheel-rail interaction model was used to determine any change in the wheel-rail contact dynamic force due to changing the rail deck and/or changing the rail isolators. The changes in dynamic force were then used to scale the inputs to the FEA/SEA model in order provide a more accurate comparison of the vibro-acoustic performance of the current and future deck designs and to calculate the change in overall noise radiated from the bridge compared to the timber deck configuration. Figure 5 shows the wheel and track dynamic FEA models.

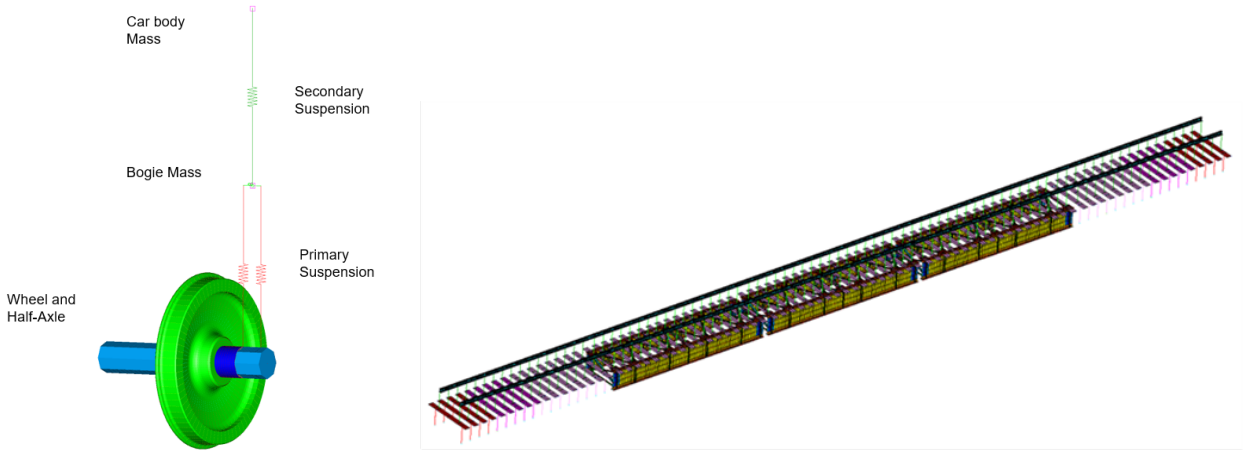

Figure 5: Wheel and track dynamic FEA models

3.2 FEA and SEA Models

The number of resonant modes of a beam or plate structure increases with increasing frequency. For a large complex structure, a dynamic FEA model becomes too large and cumbersome to process and model solution times become excessive in the high frequency regime. For structural elements in the high frequency regime where there is a high modal density, the vibration and noise radiation characteristics can be accurately modelled using space-averaged mass, stiffness and damping properties. Using these statistically averaged properties, the flow of vibration energy between coupled structures and the surrounding acoustic medium can be accurately determined. SEA models are significantly less computationally intensive compared to FEA models since noise and vibration levels are calculated in bands (typically only twenty 1/3 octave bands) to cover the 50 Hz to 4 kHz frequency range. Thus, rather than a beam or plate being described by several hundred elements in an FEA model, a beam or plate is described by a single element in an SEA model.

Recent developments in the SEA software package *VA One* enable mixed FEA/SEA models to be integrated into one model to cover a broader frequency range than would have previously been the case. A test of the number of modes in each frequency band of interest can be carried out prior to solving the model to determine which components need to be represented by finite elements and which components can be modelled using SEA. Separate FEA and SEA models solutions can then be combined.

A combined FEA/SEA model was developed using *VA One* software to examine the vibration power flow and noise radiation from the rail, transom, stringer and associated bridge truss elements covering a frequency range of 50 Hz to 4 kHz. Initially a segment of the southern approach span was modelled, which matches the segment for which test data was collected during deck mobility and operational vibration tests. Typically the FEA approach would be most appropriate below about 300 Hz and the SEA model preferred at higher frequencies. representative section of the bridge (a one stringer long section) at the southern approach was modelled incorporating the rails, rail isolators, transoms, rail deck and stringers and connected truss and girder elements. Separate models were constructed for the existing transom track form and the proposed concrete deck track form.

Figure 6 shows the SEA models of the timber transom and concrete deck versions of the southern approach span. The models were solved to determine the overall sound power output and to rank the sound power levels from subsets of structural elements (e.g. stringers, cross-girders, truss members).

An intermediate FEA/SEA result, the spatially-averaged surface vibration velocity, was compared to measurements taken during the vibration dispersion test as a means of validating/calibrating the models The vibration distribution throughout the track stringer, cross girder and support structure was compared with measurements and coupling loss factors modified in the SEA model to match measured dispersive properties of the bridge.

The sources contributing to the sound power and far field noise (1.5 m above ground level at the southern approach) were ranked based on the calibrated model of the timber transom deck. The FEA/SEA model was then updated to reflect the new concrete deck design and the model results compared to the timber transom case to quantify changes in noise sources and source ranking due to the introduction of the concrete track form.

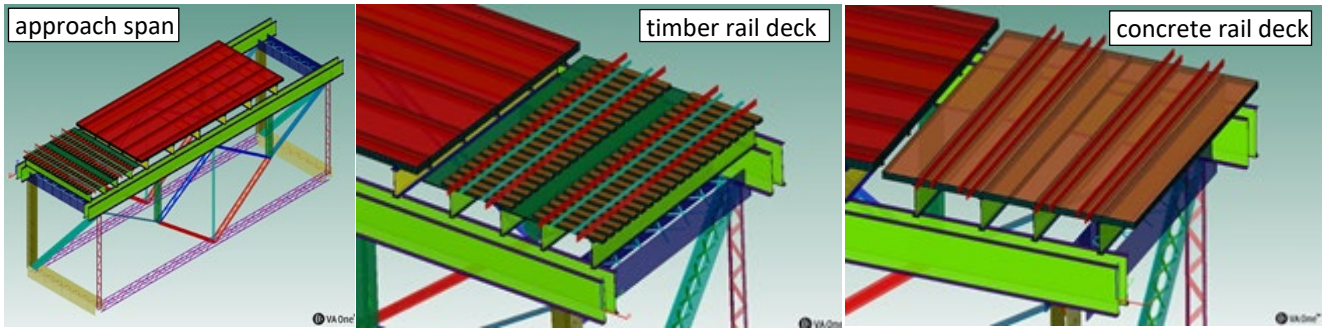

Figure 6: SEA models of the bridge (9 m long segment of approach span)

3.3 Sound Propagation Model

Once the sound power output from each of approximately 60 sources - bridge structures, rails and wheels was determined, a simple analytical model was used to calculate receiver location sound pressure levels based on the spatially distributed radiating noise sources and the influence of source-receiver geometry and shielding which is location dependent.

4 RESULTS

4.1 Rail and Wheel Receptances

Figure 7a shows the average of the rail vertical receptances midway between and directly over a transom for the timber rail deck. There are some notable differences between the measured and modelled rail receptances below 100 Hz and between 800 Hz and 1200 Hz. At low frequencies the elastic properties of the bridge structure, stringers and trusses are only approximately represented by the model due to the truncation of the FEA model below the stringer level. There are also difficulties in obtaining accurate receptance measurements at low frequencies using only a small input force during the test. The discrepancies between the model and test data at higher frequencies are due to difficulties tuning the model for the first pinned-pinned modes of rail vibration (at about 800 Hz and 1200 Hz) at which the wavelength of vibrations in the rail is equal to two/one support spacings respectively.

Figure 7b shows that the receptance from the wheel finite element model is closely matched by the receptance for a simple unsprung mass below about 100 Hz, providing a basic validation of the model. The elastic behaviour of the wheel becomes dominant over its rigid body motion above about 200 Hz and the wheel receptance is characterized by multiple natural modes of vibration, each giving rise to a distinct sharp peak in magnitude and a corresponding change of phase.

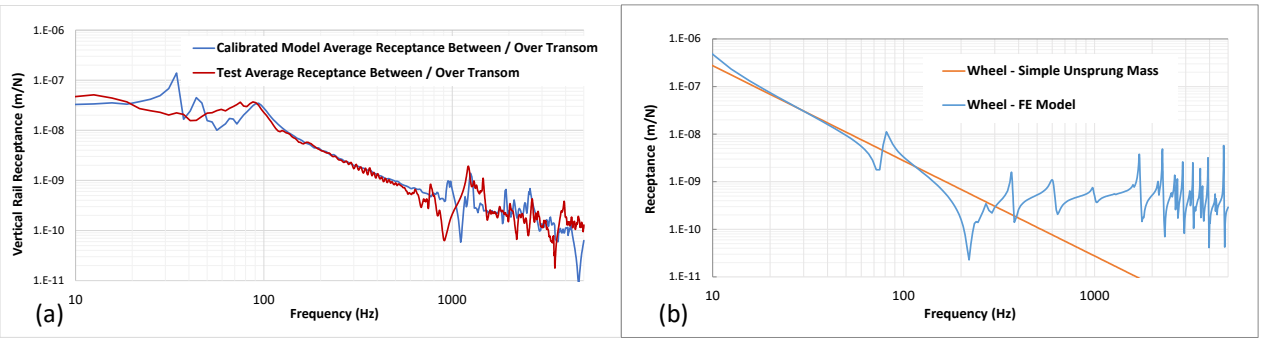

Figure 7: Rail and wheel vertical receptances

4.2 Rail Vibration and Contact Force

Point loads were applied to each rail in the vertical and horizontal directions to simulate dynamic inputs from train wheels. The forces applied to the rail were adjusted so that the simulated rail vibration matched the measured rail vibration. The resulting vertical and horizontal contact force vectors and force spectra applied to the bridge model are presented in Figure 8.

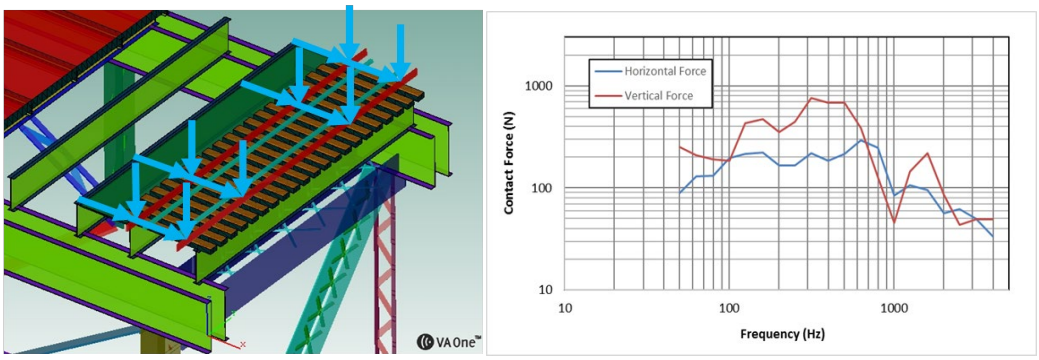

Figure 8: Point force application to rails and calculated point forces

4.3 Model Correlation

The previously determined dynamic forces were applied to the FEA/SEA model and the coupling loss factors were adjusted to match the surface averaged vibration velocity spectra measured on each element of the bridge. The FEA/SEA model predicted rail, wheel and bridge structure sound power levels and reference location sound pressure level were compared to measurements. The results presented in Figure 9 show that the overall sound power and sound pressure spectral correlation achieved between the test/analytical approach and the *VA One* FEA/SEA model was relatively strong. The individual bridge component sound power levels were similarly well correlated.

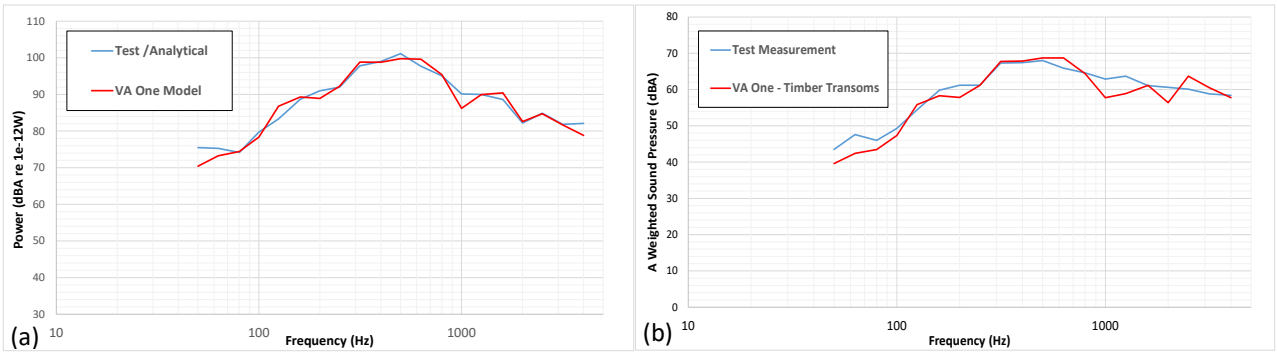

Figure 9: Test/analytical model sound power (a) and sound pressure (b) compared with FEA/SEA model results

4.4 Sound Power Ranking

The sources contributing to the sound power radiated during the constant magnitude part of the pass-by were ranked (Table 1) based on the calibrated model of the timber transom rail deck.

Table 1: Overall 'A'-weighted sound power level ranking (50 Hz – 4 kHz)

Approach span (per 9 m stringer length)			Main span (per 18 m stringer length)		
Rank	Element	'A'-weighted SWL	Rank	Element	'A'-weighted SWL
1	Stringers	101.7	1	Timber walkway	100.8
2	Timber walkway	99.2	2	Rail vertical	100.2
3	Rail vertical	97.2	3	Rail horizontal	100.0
4	Rail horizontal	97.0	4	Rail stringers	95.0
5	Guard rail	96.5	5	Cross girders	91.5
6	Transoms	94.7	6	Transoms	90.8

There are some differences in the sound power rankings between the approach span and main span. The sound power ranking of the timber walkway is higher for the main span than the approach span due to the increased surface area when compared to the approach span. The sound power contribution of the main span stringers is less than for the approach span. This may in part be due to the deeper (stiffer) stringer beams on the main span and also, the differences between the connection detail of the rail stringers to the cross girders. A review of the measured transfer receptance data for the approach and main spans indicated that the vertical vibration response of the stringer for a unit vertical force on the rail was broadly lower on the main span in comparison to the approach span, which is consistent with the results of the FEA/SEA model.

4.5 Predicted Sound Power for the New Concrete Rail Deck

The wheel-rail interaction model was used to determine the updated contact force spectra for the new concrete rail deck. The new rail deck was predicted to have a negligible influence on the wheel-rail contact forces at frequencies above 100 Hz and a significant influence below that frequency. The updated force spectra were applied to the wheel FEA model and to the FEA/SEA model of the bridge. Figure 10 shows the predicted 'A'-weighted sound power spectrum for the timber transom and concrete rail decks for a 9 m length of the approach span. The model predicts an reduction in the overall sound power level of approximately 3 dBA. The corresponding predicted reduction in the sound power level for the main span was approximately 1 dBA.

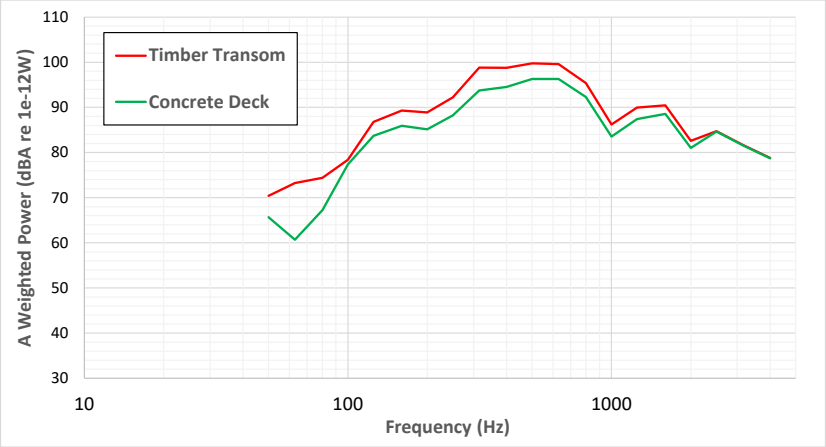

Figure 10: Predicted sound power level for timber and concrete bridge decks (approach span)

The difference in sound power due to replacing the timber transom deck with a concrete deck can be explained by considering differences between the two configurations in terms of the surface averaged mean square velocity, acoustic radiation ratios and the radiating surface areas of the rail deck elements. The net result of changes in each of the these parameters is a reduction in radiated sound power level from the rail deck.

5 CONCLUSIONS

An FEA/SEA model was used to quantify and rank the sound power contributions from rail pass-by events on the Sydney Harbour Bridge and to quantify the expected change in sound power level and sound pressure levels due to a change in the rail deck. Test data was used to quantify the combined wheel and rail roughness and contact forces to scale model parameters to achieve detailed correlation and enahnce the predictive power of the model.

ACKNOWLEDGEMENTS

The authors would like to acknowledge the assistance of Pacific ESI, for their supply and support of *VA One* SEA software and Radek Kochanowski of Sydney Trains for taking track vibration decay rate measurements.

REFERENCES

Bies D. and Hansen C. (2009). *Engineering Noise Control Theory and Practice*, 4th ed. Spon Press.

EN15461:2008+A1:2010 *Railway applications – Noise emission – Characterisation of track sections for pass by noise measurement (includes amendment A1:2010),* CEN, Brussels, Belgium.

EN15610:2009 *Railway applications – Noise emission – Rail roughness measurement related to rail rolling noise generation,* CEN, Brussels, Belgium.

Janssens M.H.A., Dittrich M.G., de Beer F.G., Jones C.J.C. (2006). "Railway noise measurement method for pass-by noise, total effective roughness, transfer functions and track spatial decay", *Journal of Sound and Vibration,* vol. 293, pp. 1007-1028. https://doi.org/10.1016/j.jsv.2005.08.070

Thompson D.J. (2008). *Railway noise and vibration: mechanisms, modelling and means of control*. Elsevier Science and Technology.